Journal of Engineering Science and Technology
Vol. 13, No. 1 (2018) 122 - 140

NUMERICAL THERMAL ANALYSIS OF SCHOTT 2008 PTR70 SOLAR RECEIVER UNDER HASSI R'MEL POWER PLANT OPERATION CONDITIONS

ABDELAALI BENIDIR[1], FOUAD KHALDI[1,*],
ABDELMOUMENE HAKIM BENMACHICHE[2], FETHI BOURAS[3]

[1]LPEA Laboratory, Department of Physics, University of Batna 1, (05000) Batna, Algeria
[2]Department of Mechanical Engineering, University of Biskra, (07000) Biskra, Algeria
[3]Department of Physics, University of El Oued, (39000) El Oued, Algeria
*Corresponding Author: fouadkhaldi@gmail.com

Abstract

The paper presents a numerical thermal analysis concerning the operation of the solar receiver Schott PTR-70 under the running conditions of Hassi R'Mel power plant. The analysis is based on numerical resolution by finite difference method of a 1D transient modelling of heat transfer balances taking place in the receiver. At first, a modelling validation against experimentally determined correlations issued from NREL facility tests is given. The comparison and confirmation are in terms of thermal efficiency and linear heat loss of the receiver versus HTF average temperature. Then, a discussion is developed about how the production of hot HTF (392°C) varies versus DNI intensity for four typical days each representative of a season? Afterwards, it is concluded that the enhancement of heat convective transfer between the absorber and the HTF would have no positive effect on HTF mass flow rate.

Keywords: Hassi R'Mel power plant, Schott PTR-70 solar receiver, Thermal 1D transient modelling, ASHRAE DNI Model, Receiver operation under transient conditions.

1. Introduction

The production of electric power by concentrating solar radiation is one of the fastest developing technologies at world level [1, 2]. Concentrating solar systems including parabolic trough collectors (PTCs) and using synthetic oil as heat transfer fluid (HTF) are the most proven, widespread and commercially tested technologies available for solar harnessing [3, 4]. Many solar power plants adopting this solar

Nomenclature

A	Cross sectional area, m^2
A_{as}	Site climate-related constant
Ac	Accommodation coefficient
A_p	Aperture area, m^2
B_{as}	Site climate-related constant
b	Interaction coefficient
C_{as}	Site climate-related constant
C_p	Specific heat, J/kg K
D	Tube diameter, m
DNI	Direct normal irradiance per unit of collector area, W/m^2
e_{da}	Dirt on receiver
e_{dm}	Dirt on mirrors
e_{ge}	Geometry error (mirror alignment)
e_{sh}	Receiver shadowing (bellows, shielding, supports)
e_{tr}	Tracking error
e_{un}	Unaccounted
$F_{cloudiness}$	Cloudiness coefficient
FR	Mass flow rate of HTF, kg/s
h	Convection heat transfer coefficient, W/m^2K
HL	Receiver heat loss, W/m
K_θ	Incidence angle modifier
k	Thermal conductivity, W/m K
L	Receiver length, m
m^i	Mass in segment ''i'', kg
N_{clear}	Number of clear days in year
N_{cloudy}	Number of cloudy days in year
n	Number of segments
n_j	Number of the day in a year
Nu	Nusselt number
P	Gas pressure, mmHg
Pr	Prandtl number
Q^i	Heat flow for receiver segment ''i'', W
Q^i_{sol}	Direct incident solar irradiance absorption rate in segment ''i'', W
Q^i_x	Heat rate coming to the segment 'i', W
$Q^i_{(x+\Delta x)}$	Heat rate leaving from the segment 'i', W
q_{sol}	Solar irradiance per receiver length, W/m
Ra	Rayleigh number
Re	Reynolds number
T	Temperature, K
t	Time, s
V	Speed, m/s
W	Collector width, m

Greek Symbols

α	Absorptance factor
γ	Molecular diameter of annulus gas, cm
Δx	Receiver segment length, m
δ	Molecular diameter of annulus gas, cm

ε	Emittance
ζ	Friction factor
η	Effective optical efficiency
η_{th}	Thermal efficiency
θ	Solar incidence angle, degree
θ_z	Solar zenith angle, degree
λ	Mean-free-path between collisions of a molecule, m
ρ	Density, kg/m^3
ρ_{cl}	Clean mirror reflectance
σ	Stefan–Boltzmann constant (5.6697×10^{-8} W/m^{2}K^4)
τ	Transmittance factor
Subscripts	
0	At design conditions
a	Absorber pipe
amb	Ambient
an	Annulus
avr	Average
conv	Convection
diff	Diffusion
e	Exterior
f	Fluid
g	Glass envelope
i	Interior
in	Inlet
loop	One loop
net	Net
out	Outlet
rad	Radiation
sky	Sky
std	Standard
w	Wind

technology are in operation [5-8]. We cite, among others, 9 units SEGS in USA, around twenty power plants in Spain, Integrated Solar Cycle System (ISCC) Hassi R'Mel in Algeria, ISCC Kuryamat in Egypt, Shams 1 in UAE, ISCC Ain Beni Mathar and Nour 1in Morocco, and ISCC Yazed in Iran.

Many research works developed physical models for studying the heat transfer characteristics and thermal performance of solar receivers, which are the major components in PTCs [4]. In these models the receiver is divided into several segments and the thermal energy balance expressed in terms of conduction/convection/ radiation mechanisms, is applied on each element, i.e., the heat transfer fluid (HTF), the absorber and the glass envelope. The obtained differential equations are computed by finite difference or finite volume numerical simulations [9-11].

The complexity of thermal modelling of receivers varies from a steady 1D model with uniform solar heat flux onto the absorber [12] to an unsteady 3D model with nonuniform heat flux [13], and many of the developed models were validated against measurement data [14]. In this research activity, optical and thermal performances of different receiver technologies are examined and

compared, i.e., Solel UVAC3, Schott 2008 PTR-70, and Schott 2011 PTR-70 [15]. Otherwise, some studies evaluated the receiver performance with various kinds of HTFs, i.e., Syltherm 800, Therminol VP-1, water, air and molten salt [16, 17]. Besides, the effects of receiver geometric parameters on the heat transfer performance were investigated [18-20]. The research work [21] compared 1D with 3D models, and showed that the 1D models still give acceptable results.

In this paper, we present a 1D transient thermal model to characterize the thermal properties of the receiver Schott 2008 PTR-70 integrated in Hassi R'Mel power plant [6]. This ISCC power plant, located in the desert of Algeria has been in operation since 2011. A particular attention is paid to how the receiver supplies hot HTF to the power block with variable climatic conditions of the Hassi R'Mel site.

2. Thermal Modelling

2.1. Energy balance model of the parabolic trough collector

In Fig. 1, a cross-section of a parabolic trough collector is represented. PTCs are made by bending a sheet of reflective surface into a parabolic shape. Typically, thermal fluid circulating through a metal black tube absorber is placed along the focal line of the receiver. The absorber is covered with a glass envelope, with vacuum or air in the space between the receiver and cover, to decrease convective heat losses.

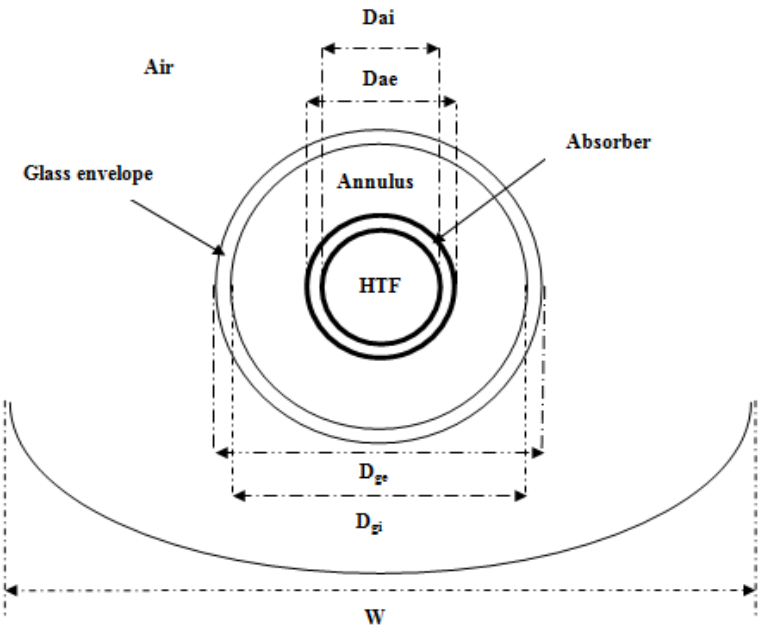

Fig. 1. Schematic of the PTC.

When the direct solar radiation is reflected by the reflector, most of this energy is absorbed by the absorber pipe which transmits this useful heat to the

fluid. The receiver model is based on an energy balance in each section of the glass envelope, absorber pipe and the fluid. Therefore, the different heat transfer coefficients must be known.

In this study, for thermal modelling it will be necessary to divide into n equal segments the receiver. In consequence, the thermal energy balances, expressed in terms of conduction/convection/ radiation mechanisms, are applied on each element of the heat transfer fluid (HTF), absorber and glass envelope. The differential equations obtained are solved with the finite difference method.

The following assumptions are considered in the mathematical modelling:

- One dimensional flow of the HTF circulating through the absorber,
- No radial heat conduction within the HTF, absorber and glass cover,
- Transient heat balance regime,
- Vacuum in the annular between absorber and glass envelope,
- The HTF is assumed to be incompressible and its physical properties vary versus temperature, and
- Constant diameters and concentrator surfaces.

2.1.1. Energy balance on the HTF

We start with the HTF heat balance. This could be expressed by a temperature differential equation [9, 10, 12, 21]. For a segment ‘‘i’’ of length Δx along the x position, the HTF partial equation is given:

$$m_f^i . C_{p_f} . \frac{dT_f^i}{dt} = Q_x^i - Q_{(x+\Delta x)}^i + Q_{f,diff}^i + Q_{f,conv}^i \tag{1}$$

From Eq. (1), the heat balance per unit of segment length is:

$$\rho_f . A_f . C_{p_f} . \frac{dT_f^i}{dt} = FR . C_{p_f} . \frac{T_f^{i-1} - T_f^i}{\Delta x} + A_f . k_f . \frac{T_f^{i+1} + 2 . T_f^i + T_f^{i-1}}{\Delta x^2} + h_f . \pi . D_{a_i} . \left(T_a^i - T_f^i\right) \tag{2}$$

with

$$A_f = \frac{\pi {D_{a_i}}^2}{4} \tag{3}$$

2.1.2. Energy balance on the absorber

For the absorber pipe the heat balance is [9, 10, 12]:

$$m_a^i . C_{p_a} . \frac{dT_a^i}{dt} = Q_{sol,a}^i + Q_{a,diff}^i - Q_{f,conv}^i - Q_{a,conv}^i - Q_{a,rad}^i \tag{4}$$

The heat balance per unit of segment length is then:

$$\rho_a . A_a . C_{p_a} . \frac{dT_f^i}{dt} = \frac{Q_{sol,a}}{L} + A_a . k_a . \frac{T_a^{i+1} + 2.T_a^i + T_a^{i-1}}{\Delta x^2} - h_f . \pi . D_{a_i} . \left(T_a^i - T_f^i\right) - h_{an} . \pi . D_{a_e} . \left(T_a^i - T_g^i\right) - \frac{\sigma \pi D_{a_e} \left(T_a^{i\,4} - T_g^{i\,4}\right)}{\left[\frac{1}{\varepsilon_a} + \left(\frac{(1-\varepsilon_g) D_{a_e}}{\varepsilon_g D_{g_i}}\right)\right]} \quad (5)$$

with

$$A_a = \frac{\pi\left(D_{a_e}{}^2 - D_{a_i}{}^2\right)}{4} \quad (6)$$

2.1.3. Energy balance on the glass envelope

The heat balance on the glass envelope leads to the next equation [9, 10, 12]:

$$m_g^i . C_{p_g} . \frac{dT_g^i}{dt} = Q_{sol,g}^i + Q_{g,diff}^i + Q_{a,conv}^i + Q_{a,rad}^i - Q_{g,conv}^i - Q_{g,rad}^i \quad (7)$$

The heat balance per unit of length is then:

$$\rho_g . A_g . C_{p_g} . \frac{dT_g^i}{dt} = \frac{Q_{sol,g}}{L} + A_g . k_g . \frac{T_g^{i+1} + 2.T_g^i + T_g^{i-1}}{\Delta x^2} + h_{an} . \pi . D_{a_e} . \left(T_a^i - T_g^i\right) + \frac{\sigma \pi D_{a_e} \left(T_a^{i\,4} - T_g^{i\,4}\right)}{\left[\frac{1}{\varepsilon_a} + \left(\frac{(1-\varepsilon_g) D_{a_i}}{\varepsilon_g D_{g_i}}\right)\right]} - h_{amb} . \pi . D_{g_e} . \left(T_g^i - T_{amb}\right) - \sigma \varepsilon_g \pi D_{g_e} \left(T_g^{i\,4} - T_{sky}{}^4\right) \quad (8)$$

with

$$A_g = \frac{\pi\left(D_{g_e}{}^2 - D_{g_i}{}^2\right)}{4} \quad (9)$$

2.2. Expression of heat transfer coefficients

2.2.1. Convection heat transfer between the HTF and the absorber

The HTF convection heat transfer coefficient h_f is given by:

$$h_f = \mathrm{Nu_f} \frac{k_f}{D_{a_i}} \quad (10)$$

The following Nusselt number correlation developed by Gnielinski [22] is used for the convective heat transfer from the receiver pipe to the HTF:

$$\mathrm{Nu_f} = \frac{\left(\zeta/8\right)(\mathrm{Re_f} - 1000)\mathrm{Pr_f}}{1 + 12.7\sqrt{\zeta/8}\left(\mathrm{Pr_f}^{\frac{2}{3}} - 1\right)} \quad (11)$$

with

$$\zeta = (1.82 \log_{10}(\mathrm{Re_f}) - 1.64)^{-2} \quad (12)$$

2.2.2. Convection heat transfer coefficient for the annulus gas

To determine the convection heat transfer coefficient between the absorber and the glass envelope, we suppose the receiver annulus is under vacuum (Pan ≤ 100 mmHg). The convection heat transfer between the absorber and the glass envelope occurs by free-molecular convection [23]. Then, we have:

$$h_{an} = \frac{k_{std}}{\frac{D_{a_e}}{2\,ln\left(\frac{D_{g_i}}{D_{g_e}}\right)} + b\,\lambda\left(\frac{D_{a_e}}{D_{a_i}} + 1\right)} \tag{13}$$

For

$$Ra_{an} < \left(\frac{D_{g_i}}{D_{g_i} - D_{a_e}}\right)^4 \tag{14}$$

and

$$b = \frac{(2 - ac)(9\gamma - 5)}{2\,ac\,(\gamma + 1)} \tag{15}$$

and

$$\lambda = \frac{2.331 \times 10^{-20} T_{avr}}{(P_{an}\delta^2)} \tag{16}$$

with:

$$T_{avr} = \frac{\left(T_a + T_g\right)}{2} \tag{17}$$

2.2.3. Convection heat transfer coefficient for air ambient

If there is wind, the convection heat transfer is forced convection. The correlation developed by Zhukauskas is used to estimate the Nusselt number [9, 23]:

$$\overline{\mathrm{Nu}}_{\mathrm{amb}} = 0.26\,\mathrm{Re}_{\mathrm{amb}}{}^{0.6}\,\mathrm{Pr}_{\mathrm{amb}}^{0.37}\left(\frac{\mathrm{Pr}_{\mathrm{amb}}}{\mathrm{Pr}_{\mathrm{g}}}\right)^{\frac{1}{4}} \tag{18}$$

2.2.4. Internal and external radiation heat transfer coefficients

The internal and external radiation heat transfer coefficients are calculated by Stefan Boltzmann's law [10]

$$h_{rad_e} = \varepsilon_g \sigma\left[{T_{sky}}^2 + {T_g}^2\right]\left(T_{sky} + T_g\right) \tag{19}$$

and

$$h_{rad_i} = \varepsilon_i \sigma\left[{T_a}^2 + {T_g}^2\right]\left(T_a + T_g\right) \tag{20}$$

where

$$\varepsilon_i = \frac{D_{g_i} / D_{a_e}}{\frac{1}{\varepsilon_a} + \frac{1-\varepsilon_g}{\varepsilon_g}} \tag{21}$$

2.3. Numerical resolution and algorithm

An explicit scheme is used to discrete the transient terms, whereas the 1st order upwind scheme and the 2nd central scheme are used for the spatial discretization. The obtained system of three ordinary differential equations is solved using the 4th order Runge Kutta method. To this end, a global algorithm (as shown in Fig. 2), developed under MATLAB environment, is used with the following points: i) the physical properties including the density, specific heat, dynamic viscosity, and thermal conductivity of the HTF are calculated as functions of temperature, ii) ambient conditions include wind speed, ambient temperature, zenith angle, azimuth angle for the site of Hassi R'Mel are obtained from the database of Meteonorm [24], and iii) the characteristics of the PTC integrated in the Hassi R'Mel power plant are reported in Table 1.

Table 1. Characteristics of the solar receiver.

Designation	Specifications
Receiver type	SCHOTT PTR-70 2nd generation
Absorber internal diameter (m)	0.066
Absorber external diameter (m)	0.07
Glass cover internal diameter (m)	0.114
Glass cover external diameter (m)	0.12
Absorber material type	304L
HTF type	THERMINOL VP-1 [25]
HTF density (kg/m^3)	-0.90797 T (°C) + 0.00078116 T^2 (°C) - 2.367 10^{-6} T^3(°C) + 1083.25
HTF specific heat (kJ/kg K)	0.002414 T (°C) + 5.9591 10^{-6} T^2 (°C) – 2.9879 10^{-8} T^3 (°C) + 1.498
HTF thermal conductivity (W/m K)	-8.19477 10^{-5} T (°C) -1.92257 10^{-7} T^2 (°C) + 2.5034 10^{-11} T^3(°C) +0.137743
HTF kinematic viscosity (mm^2/s)	$e^{([544.149/\ (T\ (°C)+114.43)]-2.59578)}$
Thermal conductivity of absorber pipe (W/m K)	0.0153 T_a+14.8 [23]
Density of absorber pipe (kg/m^3)	8020
Specific heat of glass envelope (J/kg K)	1090
Density of glass envelope (kg/m^3)	2230
Radiation emissivity of glass envelope (-)	0.89
Radiation emissivity of absorber (-)	0.062+2 10^{-7} T_a^2 [26]

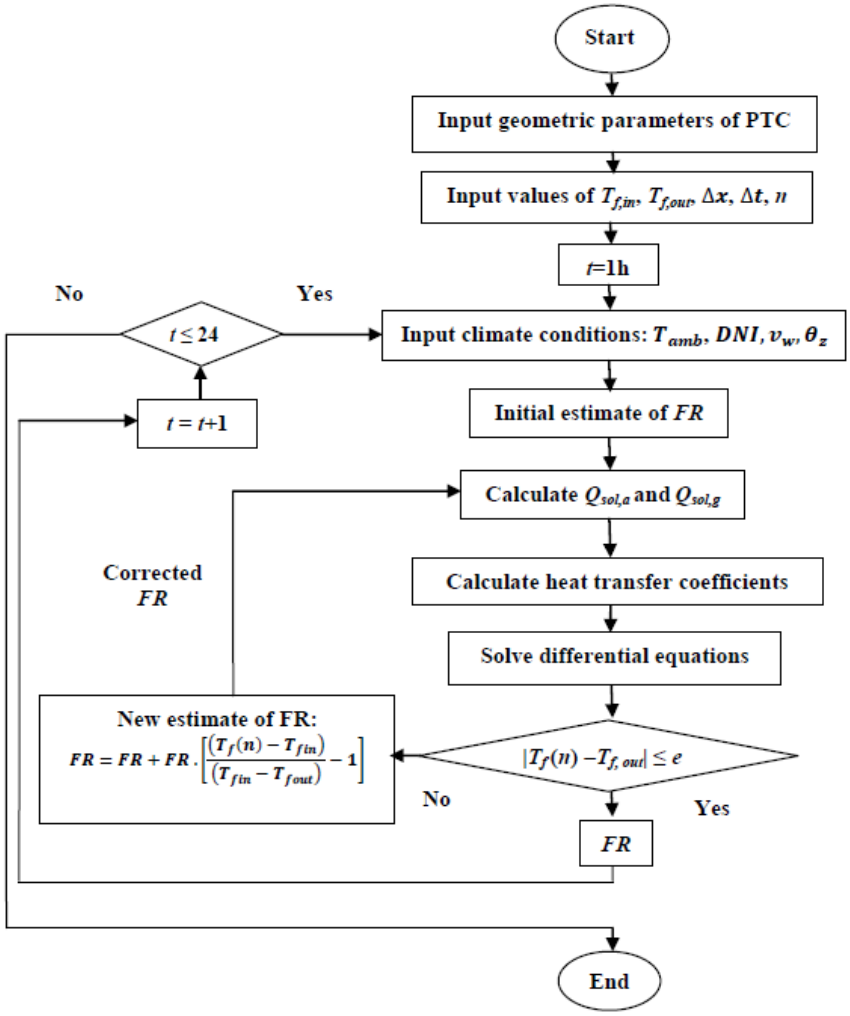

Fig. 2. Algorithm for numerical calculation of HTF mass flow rate.

2.4. Estimation of solar energy absorption

The energy absorbed by the glass envelope is [20, 23]:

$$Q_{sol,g} = DNI \,.\cos(\theta)\,.A_p.\eta_g.\alpha_g \tag{22}$$

where

$$A_p = W.L \tag{23}$$

and

$$\eta_g = e_{sh}e_{tr}e_{da}e_{ge}e_{dm}e_{un}\rho_{cl}K_\theta \tag{24}$$

The heat flux absorbed by the absorber pipe is [20, 23]:

$$Q_{sol,a} = DNI \,.\cos(\theta)\,.A_p.\eta_a\ \ \alpha_a \tag{25}$$

with

$$\eta_a = \eta_g\ \tau_g \tag{26}$$

and the incident angle modifier K_θ is estimated by:

$$K_\theta = 1 + 1.06 \times 10^{-4}\ \ \theta - 1.709 \times 10^{-4}\ \theta^2 \tag{27}$$

The direct normal radiation DNI is determined using the ASHRAE model [27, 28]. The choice of this model is well argued. Indeed, by comparison to ground measured data of an Algerian site very close to Hassi R'Mel site, the ASHRAE model has the best estimation of the DNI among many examined models [27]. The DNI is calculated by a simple formula:

$$DNI = A_{ash}\mathrm{EXP}\left(-\frac{B_{ash}}{\cos(\theta_z)}\frac{p}{p_0}\right)\cos(\theta_z) \tag{28}$$

The symbols A_{as}, B_{as} and C_{as} can be estimated using the following equations:

$$DNI = A_{ash}\mathrm{EXP}\left(-\frac{B_{ash}}{\cos(\theta_z)}\frac{p}{p_0}\right)\cos(\theta_z) \tag{28}$$

$$A_{ash} = 1140 + 75\cos\left(F_{cloudiness}n_j\right) \tag{29}$$

$$B_{ash} = 0.132 + 0.023\cos\left(F_{cloudiness}n_j\right) \tag{30}$$

and

$$C_{ash} = 0.047 + 0.03\cos\left(F_{cloudiness}n_j\right) \tag{31}$$

where

$$F_{cloudiness} = 1 - \frac{N_{jcloudy}}{N_{jclear}} \tag{32}$$

3. Case Study: PTR-70-2008 Receiver

The solar receiver under examination in the present study is the PTR-70-2008 model. This technology is integrated into the first Algerian Integrated Solar Combined Cycle (ISCC) power plant [6]. This power plant began to run in 2011. At 183,120 m^2 of mirrors, the solar field, designed with a solar multiple of 2, comprises 224 ET-150 collectors assembled in 56 loops, 4 collectors per loop. The PTR-70-2008 solar receiver is conceived to run with Therminol PV-1 as a HTF. The collectors are aligned on a north-south line. They track sun from east to west by a single axis sun tracking system. The solar field is sized to supply, at DNI=751 W/m^2, 100 MW of thermal energy at 392°C to the block power. However, with the conception of Hassi R'Mel power plant at nominal regime the solar field is supposed to run only on a half of its design capacity, it supplies then 50 MW of thermal energy to the power plant.

The operation of the solar field is under the compulsory condition that the HTF circulates across each loop at constant inlet temperature, 293°C, and at

constant outlet temperature, 393°C. However, the HTF mass flow rate varies following the DNI intensity. The design value of the HTF mass flow rate is 7.33 kg/s per one loop. It is the resultant of DNI assumed at 751 W/m^2. This estimation is the yearly average value of DNI striking the site of Hassi R'Mel. Therefore, at nominal operating regime of the Hassi R'Mel power plant the HTF mass flow rate is 3.66 kg/s per loop.

With a solar-to-electricity efficiency of about 17%, the solar energy share in the full capacity of the plant (160 MW) is about 14% (22 MW).

The site of Hassi R'Mel power plant is located in middle of Algeria, at about 500 km from Algiers. It is at 33°7' latitude and 3°21'longittude, and its elevation above sea level is 750 m. The ambient temperature ranges between 21°C and 50°C in summer and ranges between -10° C and 20°C in winter. In summer, the Direct Normal Irradiation (DNI) can reach a maximum intensity of 930 W/m^2.

It is common that the thermal performance of any solar receiver is characterized experimentally in terms of thermal efficiency and linear heat loss versus average HTF temperature [29]. Experimentally determined correlations issued from NREL facility tests for these two parameters are given for the receiver PTR-70 2008 [26].

The linear heat loss (W/m) can be calculated by the following correlation:

$$L = 4.05 + 0.247\left(T_f - T_{amb}\right) \pm 0.00146\, T_f^2 + 5.65\text{E} - 06\, T_f^3 + 7.62\text{E} - 08\, DNI\, K_\theta\, cos(\theta)\, T_f^2 + \sqrt{V_w}\left[-1.70 + 0.0125\left(T_f - T_{amb}\right)\right] \quad (33)$$

The thermal efficiency is estimated by the following empirical formulation:

$$\eta_{th} = {}^{Q_{net_{\Delta X}}}/_{q_{sol}} \quad (34)$$

with

$$q_{sol} = DNI\, A_p \quad (35)$$

An empirical correlation is obtained to calculate the mass flow rate of HTF produced by one loop:

$$FR_{loop} = {}^{Q_{net_{loop}}}\Big/_{C_{p_{loop}}(T_{out} - T_{in})} \quad (36)$$

4. Results and Discussion

4.1. Modelling validation against NREL facility tests

It is common that the thermal performance of any solar receiver is characterized experimentally in terms of thermal efficiency and linear heat loss versus average HTF temperature [29]. Experimentally determined correlations issued from NREL facility tests for these two parameters are given for the receiver PTR-70 2008 [26]. The two parameters, computed in the present study and that issued from empirical correlations [26] are displayed and compared in Figs. 3 and 4, respectively. A first result is that the computed and determined experimentally quantities are similar and have almost the same trends. This is a first validation of

the numerical modelling applying in the present study. From those figures, it appears also that when the temperature of the HTF varies from 290 to 380°C the thermal efficiency of the receiver decreases from 0.66 and 0.69. This trend is associated to an increase of heat loss from 90.5 W/m to 195 W/m. On average, for every 1°C increase in HTF temperature the thermal efficiency of the PTR 70 receiver decreases by 0.04%.

As a conclusion, the thermal performance of the receiver decreases because HTF temperature rising augments the absorber heat loss by thermal radiation. The explanation is based on Fig. 5 which presents the temperature rise of the HTF, the absorber and the glass envelope along one loop (600 m) at design value of DNI (751 W/m^2). At first, we confirm the quasi-equality of design fixed value [6] and computed value by the present study of HTF mass flow rate, 7.33 and 7.34 kg/s, respectively. The temperature rise trends for all the three elements are almost linear. The temperature rise per meter of the HTF is about 0.18°C at the loop inlet and it is 0.14°C at the loop outlet. Indeed, the net gain of energy decreases as the fluid progresses through the loop because heat loss increases as the HTF temperature increases. The absorber is hotter than the HTF along the loop by on average 4°C, while the temperature of the glass envelope is below than that of the absorber by on average 238°C.

This disparity in temperature differences between the three components of the receiver is the consequence from the fact that thermal resistances between these three elements are different. For example, at design conditions the flow regime is turbulent (Re=354690), the convective thermal resistance between the absorber and the HTF is about 0.0106 W/°C, and the radiative thermal resistance between the absorber and the glass envelope is much greater, it is around 25 W/°C. By connecting between Fig. 4 and Fig. 5 we can deduce that the mean heat loss in the first collector is 120 W/m, in the second collector it is 150 W/m, in the third collector it is 172 W/m, and in the fourth and last collector the mean heat loss is 214 W/m. It comes out that the fourth and last receiver is the subject of higher temperature and in consequence is the source of higher heat loss by thermal radiation

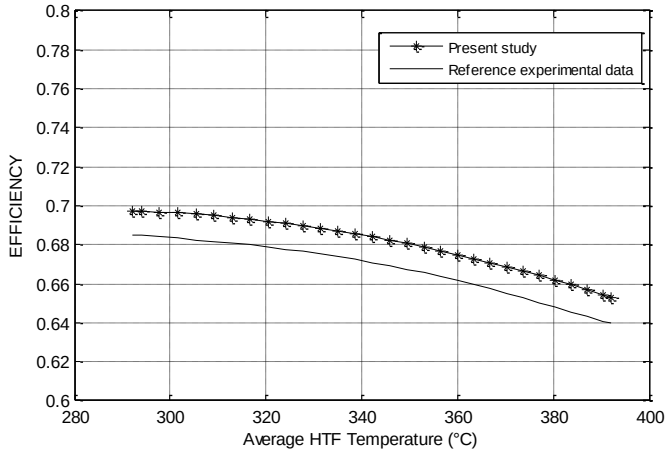

Fig. 3. Receiver thermal efficiency: comparison between computed (present study) and measured results [26].

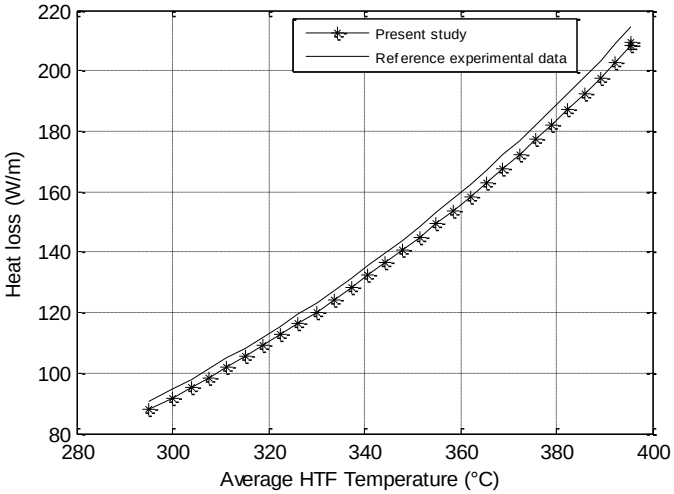

Fig. 4. Receiver linear thermal loss: comparison between computed (presented study) and measured results [26].

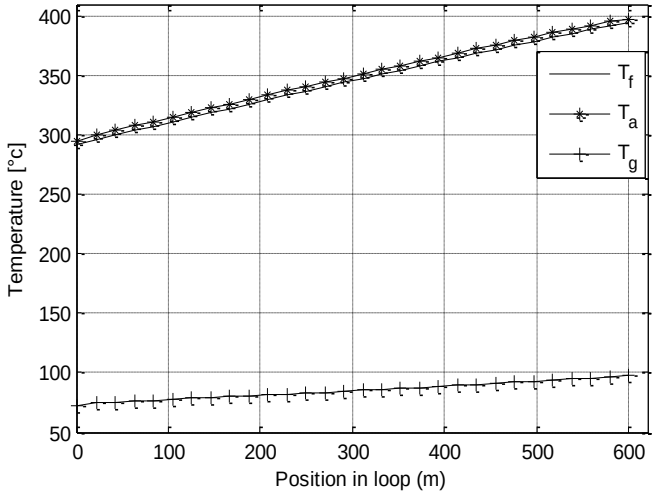

Fig. 5. Variation of temperature along position in one loop at design conditions, for the HTF, absorber, and glass envelope.

4.2. Hourly production of HTF mass flow rate

At first, the hourly variations of DNI intensity on the site of Hassi R'Mel are computed, based on the ASHRAE model, for four typical days of a year. These typical days, representative each a season, are: spring equinox on the 21st of March, summer solstice on the 21st of June, autumnal equinox on the 21st of September, and winter solstice on the 21st of December. The results are depicted in Fig. 6. The 21st of June is the sunniest day while the 21st of December is the less sunny day, in terms of DNI intensity and sunny hours. On the 21sts of Mars

and September the DNI are similar with for both a maximum of DNI exceeding 810 W/m^2. Over the four days the maximum of DNI, 950 W/m^2, is obtained on June while the smallest maximum, 520 W/m^2, is registered on the 21st of December. On Hassi R'Mel site, the sun's ray strikes the Earth 13 hours in June 21, 11 hours on Mars 21 and September 21, and 9 hours on December 21.

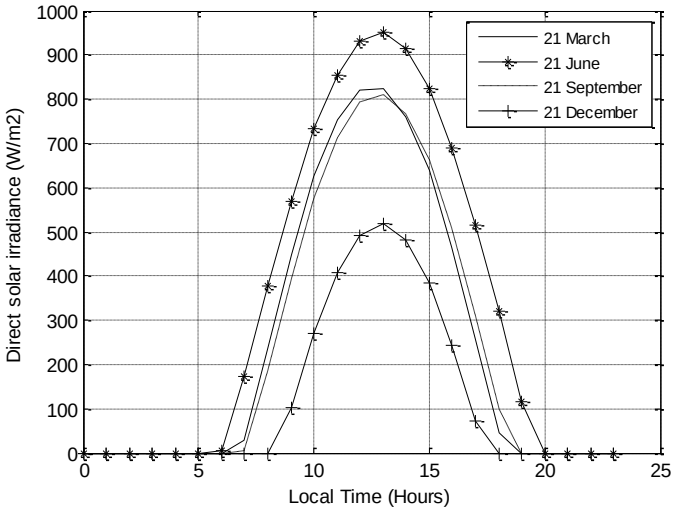

Fig. 6. Hourly variations of DNI at Hassi R'Mel site for 4 typical days.

Figure 7 shows hourly variations of HTF mass flow rate versus DNI for the four typical days of the year, the 21sts of Mars, June, September and December. The algorithm of numerical calculations of HTF mass flow rate is depicted in Fig. 2. In the figures there are comparisons of computed results by the present study against reference empirically obtained data issued from NREL facility tests [26]. According to these graphs, it appears clearly that for all considered days the results of the present modelling are in perfect agreement with experimentally fitted data.

According to these results, the HTF mass flow rate varies from 1 to 9.16 kg/s on June 21, from 0.08 to 5.65 kg/s on September and Mars 21s together, and it varies from 0.65 to 1.52 kg/s on December 21. However, actually, the operation of the solar field is under the condition that the HTF mass low rate must be within an interval delimited by a minimum and a maximum. On one hand, the minimum is dictated by the fact that the HTF circulates in the PTCs always and only in a turbulent flow regime, in order to have best conditions for convective heat transfer between the absorber and the HTF. On the other hand, the maximum HTF mass flow rate in the solar field cannot exceed the maximum capacity of HTF pumps. According to the PTR-70 receiver specifications the minimum HTF mass flow rate is around 1.8 kg/s per loop, and according to the size of pumping system installed in the solar field of Hassi R'Mel power plant, the maximum of total HTF mass flow rate circulating in the whole solar field is fixed at about 411 kg/s [6] (around 7.33 kg/s per loop). This is in relation to the fact that the solar multiple of Hassi R'Mel power plant is fixed at 2, meaning that the solar field can operate to twice its nominal capacity, which is less than 3.66 kg/s of HTF mass flow rate per loop.

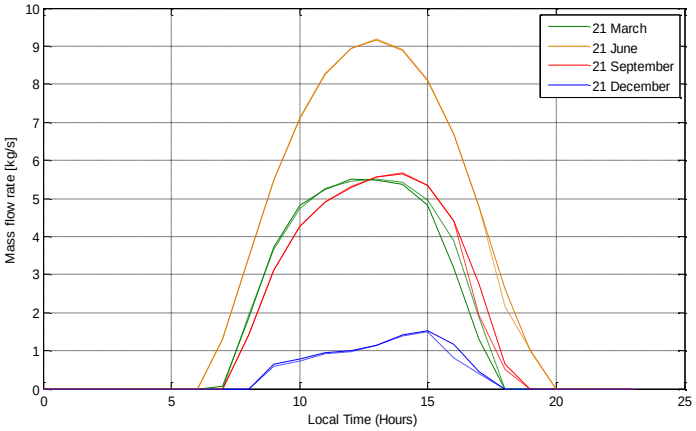

Fig.7. Hourly variation of HTF mass flow rate versus DNI for 4 typical days: comparisons between computed (present study, in continued line) and empirically predicted results [26] (dashed line).

In regard to above technical constraints, on the 21st of June the solar field operates 11 hours by supplying hot HTF at 393°C to the power block from 08h:00 to 18h:00. At 07h:00 the HTF mass flow rate is 1.32 kg/s and at 19h:00 it is 1kg/s, both values are lower the minimum limit (1.8 kg/s). In these conditions, the solar field does not supply HTF to the power block. From 11h:00 to 15h:00 the production of HTF exceeds the maximum limit (7.33 kg/s per loop). During this period of day, the solar field reaches its maximum capacity and supplies the same quantity of HTF (7.33 kg/s per loop) to the power block. In other words, the whole solar field (a total of 56 loops) supplies 411 kg/s of HTF to the power block carrying then approximately more than 100 MW of thermal energy. This operation is realized by defocusing some of PTCs. For the 21st's of Mars and September, the hourly productions of hot HTF are very similar. The solar field starts to product, per loop, more than 3 kg/s of hot HTF at 9h:00 and finishes by a HTF mass flow rate between 2.8 and 3.2 kg/s at 17h:00 (9 hours of operation). The quantity of HTF does not exceed in any hour the capacity of HTF pumps.

On the 21st of December, the poorest day in solar energy resources, the solar field does not run all the day. Its production of HTF does not exceed the minimum limit required to enable the thermal energy transfer between the solar field and the power block.

4.3. Effect of absorber heat convection coefficient on HTF mass flow rate

At design operating conditions the heat exchange between the absorber and the HTF takes place in a turbulent flow regime with a convective heat coefficient of about 2374 W/m^2.K. With this value of heat coefficient, the HTF mass flow rate per loop is 3.66 kg/s. It would be interesting to estimate the effect of increasing the value of heat coefficient on HTF mass flow rate. This investigation cannot be done with empirical models issued from experimental tests [26]. Indeed, these models are obtained at certain fixed physical and geometric parameters of the

solar receiver. In regard to numerical simulation it does not matter how the enhancement of convective heat transfer through the absorber may be. It could be by any means, i.e., geometric modification, some additive in the HTF, etc. Figure 8 illustrates how increasing the value of heat coefficient even until 20 times the value of the heat coefficient at design conditions (DNI=751 W/m^2) does not have any effect on mass flow rate of the HTF.

The explanation is as follows. The absorber transmits heat flux resulting from absorbing solar radiation into two opposite directions. It transmits an amount of heat flux (utile) to the HTF by convection and transmits some heat flux (lost) to glass envelope essentially by radiation. The radiative thermal resistance is very largely higher to the convective thermal resistance (25 against 0.0106 W/°C), and then increasing the convective coefficient until 20 times does not affect the dominance of radiative thermal resistance on convective thermal resistance. In other words, the balance between convection in one direction and thermal radiation in other direction remains unchanged; as a consequence, the convective heat flux is the same, and the HTF mass flow rate is the same. As a result, there no effect of enhancing convective heat transfer through the absorber pipe on the receiver performance when the current design of the receiver is kept unchanged, i.e., dimensions, HTF mass flow rate, etc. It should necessary then to reconsider the whole design of the receiver to integrate any new means for enhancing the heat transfer in the absorber.

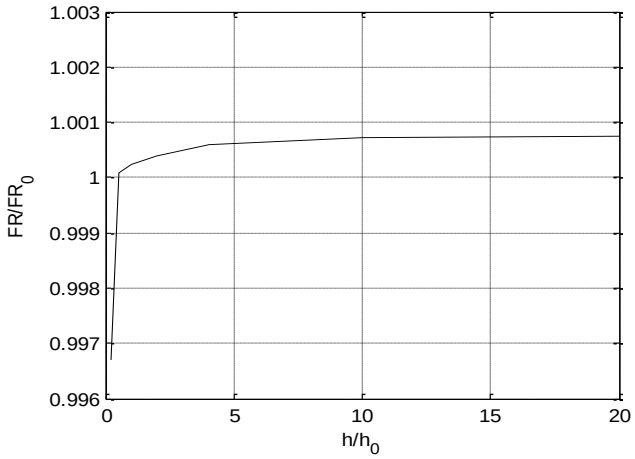

Fig. 8. HTF mass flow rate versus heat transfer coefficient through the absorber.

5. Conclusion

The purpose of this study is a thermal analysis about the operating of the solar field of Hassi R'Mel power plant. The analysis is based on numerical simulation of transient heat transfer balance on each of the three components of the receiver, the heat transfer fluid, absorber and glass envelope. The calculations consider one loop (600 m), which is the alignment of four ET-150 collectors. The results of the study are in very fair agreement with experimental characterization performed on the solar receiver PTR-70 in NREL facility tests. The operation of the solar field

is subjected to both climatic conditions and design constraints. The results of calculations show the following. The solar field does not run completely along a winter day. The DNI intensity does not permit the production of sufficient HTF mass flow rate needed to exceed the minimum limit. In autumn and spring days the solar field runs almost in a similar manner. It operates 09 hours without exceeding the maximum limit of HTF mass flow rate. In a summer day the solar field operates 11 hours, with 5 hours in defocusing mode in order to not exceed the maximum limit of HTF mass flow rate.

The study demonstrates that simulating an enhancement of heat transfer in the absorber by increasing the value of heat transfer convection without changing any other parameter does not have any positive effect on the conversion of solar radiation to the production of hot HTF. As a perspective, further calculations and detailed analysis will be performed in attempt to propose new means for enhancing the performance of the solar receiver; a particular attention will be paid to the last collector in the loop which is the less efficient collector.

References

1. Zhang, H.; Baeyens, J.; Degrève, J.; and Cacères, G. (2013). Concentrated solar power plants: Review and design methodology. *Renewable and Sustainable Energy Reviews*, 22, 466-481.
2. Khan, J.; and Arsalan, M.H. (2016). Solar power technologies for sustainable electricity generation–A review. *Renewable and Sustainable Energy Reviews*, 55, 414-425.
3. Fernández-García, A.; Zarza, E.; Valenzuela, L.; and Pérez, M. (2010). Parabolic-trough solar collectors and their applications. *Renewable and Sustainable Energy Reviews*, 14, 1695-1721.
4. Behar, O.; Khellaf, A.; and Mohammedi, K. (2013). A review of studies on central receiver solar thermal power plants, *Renewable And Sustainable Energy Reviews*, 23, 12-39.
5. Tsikalakis, A.; Tomtsi, T.; Hatziargyriou, N.; Poullikkas, A.; Malamatenios, C.; Giakoumelos, E.; Jaouad, O.C.; Chenak, A.; Fayek, A.; and Matar, T. (2011). Review of best practices of solar electricity resources applications in selected Middle East and North Africa (MENA) countries. *Renewable and sustainable energy reviews*, 15, 2838-2849.
6. Khaldi, F. (2012). Energy and exergy analysis of the first hybrid solar-gas power plant in Algeria. *Proceedings of ECOS 2012 - the 25th International Conferenceon* .Perugia, Italy, 26-29.
7. Behar, O.; Khellaf, A.; Mohammedi, K.; and Ait-Kaci, S. (2014). A review of integrated solar combined cycle system (ISCCS) with a parabolic trough technology. *Renewable and Sustainable Energy Reviews*, 39, 223-250.
8. Alqahtani, B.J.; and Patiño-Echeverri, D. (2016). Integrated solar combined cycle power plants: Paving the way for thermal solar. *Applied Energy*, 169, 927-936.
9. Ouagued, M.; Khellaf, A.; and Loukarfi, L. (2013). Estimation of the temperature, heat gain and heat loss by solar parabolic trough collector under

Algerian climate using different thermal oils. *Energy Conversion and Management*, 75, 191-201.

10. Marif, Y.; Benmoussa, H.; Bouguettaia, H.; Belhadj, M.M.; and Zerrouki, M. (2014). Numerical simulation of solar parabolic trough collector performance in the Algeria saharan region. *Energy Conversion and Management*, 85, 521-529.
11. Hachicha, A.A.; Rodríguez, I.; Capdevila, R.; and Oliva, A. (2013). Heat transfer analysis and numerical simulation of a parabolic trough solar collector. *Applied Energy*, 111, 581-592.
12. Padilla, R.V.; Demirkaya, G.; Goswami, D.Y.; Stefanakos, E.; and Rahman, M.M. (2011). Heat transfer analysis of parabolic trough solar receiver. *Applied Energy*, 88, 5097-5110.
13. Wu, Z.; Li, S.; Yuan, G.; Lei, D.; and Wang, Z. (2014). Three-dimensional numerical study of heat transfer characteristics of parabolic trough receiver. *Applied Energy*, 113, 902-911.
14. Liang, H.; You, S.; and Zhang, H. (2015). Comparison of different heat transfer models for parabolic trough solar collectors. *Applied Energy*, 148, 105-114.
15. Lei, D.; Li, Q.; Wang, Z.; Li, J.; Li, J.; and Li, J. (2013). An experimental study of thermal characterization of parabolic trough receivers. *Energy Conversion and Management*, 69, 107-115.
16. Zaversky, F.; Medina, R.; García-Barberena, J.; Sánchez, M.; and Astrain, D. (2013). Object-oriented modeling for the transient performance simulation of parabolic trough collectors using molten salt as heat transfer fluid. *Solar Energy*, 95, 192-215.
17. You, C.; Zhang, W.; and Yin, Z. (2013). Modeling of fluid flow and heat transfer in a trough solar collector. *Applied Thermal Engineering*, 54, 247-254.
18. Valenzuela, L.; López-Martín, R.; and Zarza, E. (2014). Optical and thermal performance of large-size parabolic-trough solar collectors from outdoor experiments: A test method and a case study. *Energy*, 70, 456-464.
19. Wang, P.; Liu, D.Y.; and Xu, C. (2013). Numerical study of heat transfer enhancement in the receiver tube of direct steam generation with parabolic trough by inserting metal foams. *Applied Energy*, 102, 449-460.
20. Behar, O.; Khellaf, A.; and Mohammedi, K. (2015). A novel parabolic trough solar collector model – Validation with experimental data and comparison to Engineering Equation Solver (EES). *Energy Conversion and Management*, 106, 268-281.
21. García-Valladares, O.; and Velázquez, N. (2009). Numerical simulation of parabolic trough solar collector: Improvement using counter flow concentric circular heat exchangers. *International Journal of Heat and Mass Transfer*, 52, 597-609.
22. Incropera, F.P.; DeWitt, D.; Bergman, T.L.; and Lavine, A.S. (2007). *Fundamentals of Heat and Mass Transfer* (6th ed.). New York: John Wiley and Sons.
23. Kalogirou, S.A. (2012). A detailed thermal model of a parabolic trough collector receiver. Energy, 48, 298-306. Meteonorm. (2005). Global meteorological database. Version 5.1. From www.meteonorm.com

24. Therminol-VP1. (2014). Technical Bulletin. Retrieved December 12, 2014, from http://www.therminol.com.
25. Burkholder, F.; and Kutscher, C.F. (2009). Heat loss testing of Schott's 2008 PTR70 parabolic trough receiver. *NREL*/TP-550-45633.
26. Behar, O.; Khellaf, A.; Mohammedi, K. (2015). Comparison of solar radiation models and their validation under Algerian climate – The case of direct irradiance. *Energy Conversion and Management*, 98, 236-251.
27. Gueymard, C.A. (2012). Clear-sky irradiance predictions for solar resource mapping and large-scale applications: Improved validation methodology and detailed performance analysis of 18 broadband radiative models. *Solar Energy*, 86, 2145-2169.
28. Forristall, R. (2003). Heat transfer analysis and modeling of a parabolic trough solar receiver implemented in engineering equation solver. *NREL*/TP-550e34169.